THE JOURNAL OF PHYSICAL CHEMISTRY C

pubs.acs.org/JPCC Article

Strongly Enhanced Dielectric Response and Structural Investigation of (Sr^{2+}, Ge^{4+}) Co-Doped CCTO Ceramics

Jakkree Boonlakhorn, Narong Chanlek, Prasit Thongbai, and Pornjuk Srepusharawoot*

Cite This: *J. Phys. Chem. C* 2020, 124, 20682−20692 Read Online

ABSTRACT: A solid−state reaction method was used to prepare (Sr^{2+}, Ge^{4+}) co-doped $CaCu_3Ti_4O_{12}$ ceramics. A single-phase of $CaCu_3Ti_4O_{12}$ was detected in all the ceramics. An enormous evolution of grain growth in (Sr^{2+}, Ge^{4+}) co-doped $CaCu_3Ti_4O_{12}$ ceramics was observed, which was due to a liquid phase sintering mechanism. Theoretical calculations showed that Ge dopant ions are more likely substituted in Cu sites rather than Ti sites. High dielectric permittivity, ∼69,889, with a low dielectric loss tangent, ∼0.038, was achieved in a $Ca_{0.95}Sr_{0.05}Cu_3Ti_{3.95}Ge_{0.05}O_{12}$ ceramic. Furthermore, dielectric permittivity at 1 kHz of this ceramic is more temperature-stable than that of the $CaCu_3Ti_4O_{12}$ and $Ca_{0.95}Sr_{0.05}Cu_3Ti_4O_{12}$ ceramics. The enhanced dielectric permittivity with reduced loss tangent in the co-doped ceramics originated from a metastable insulating phase created by a liquid phase sintering mechanism. The local insulating phase along the grain boundary layers can increase the grain boundary resistance as well as the conduction activation energy of the grain boundaries, resulting in a decreased dielectric loss tangent. An internal barrier layer capacitor model supports the origin of the giant dielectric properties in $CaCu_3Ti_4O_{12}$-based ceramics by all results in this work.

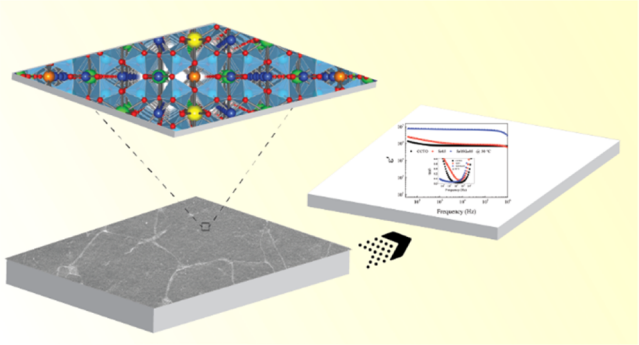

1. INTRODUCTION

The electronic properties of materials have received attention for study and improvement of their specific behavior for use in various applications. Much research has attempted to expand knowledge in several fields as reported in the literature.[1−16] Dielectric properties of advanced ceramics have been extensively investigated in various reports.[1,3−12] The $CaCu_3Ti_4O_{12}$ (CCTO) ceramic is one of the most important materials under study over the past decade. Its giant dielectric properties and nonlinear electrical response[1−12] have been widely attracting various researchers owing to its high dielectric permittivity (ε') ∼ 10^4 with no ferroelectric behavior.[11] This remarkable point promotes CCTO ceramics as a potential ceramic for use in capacitor applications. The origins of the giant dielectric properties of the CCTO ceramic have been unclear until now. Several dielectric models have been proposed to explain the dielectric properties of this dielectric ceramic. In a natural state, for example, at room temperature, a model that has been accepted as the primary origin of the giant dielectric response in the CCTO ceramic is the internal barrier layer capacitor (IBLC) model.[1,2,5,12,13] In the foundation studies of Sinclair et al.,[12] a heterogeneous microstructure was found in the CCTO ceramic. Semiconducting grains and insulating grain boundaries (GBs) reported in this work were classified using impedance spectroscopy. Additionally, the work of Chung et al.[13] supports the results of Sinclair et al. The relationship between current (I) and voltage (V) exposed by Chung et al. shows the different electrical states of grains and GBs, which are semiconducting and insulating regions, respectively.[13] In addition to confirmation of the IBLC effect in CCTO ceramics, the results of Chung et al. illustrate that the nonlinear electrical properties of these ceramics can be developed for use in other applications, such as in varistors.[14] The giant dielectric response in CCTO ceramics is acceptably described by the IBLC model. In other environments, for example, at high temperature or under a DC bias, a sample-electrode contact is dominant.[10,15] In some cases, the intrinsic factor is more dominant than the extrinsic structural factors in determining the dielectric properties of CCTO ceramics such as Zn^{2+}-doped[17] and Mg^{2+}-doped CCTO.[18]

Although the origins of the giant dielectric response in CCTO ceramics have been thus unclear, improvement of dielectric properties and electrical response of this ceramic have been continuously achieved.[1−10] The first severe problem,

Received: May 19, 2020
Revised: August 21, 2020
Published: August 28, 2020

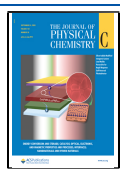

https://dx.doi.org/10.1021/acs.jpcc.0c04484
J. Phys. Chem. C 2020, 124, 20682−20692

namely, a high loss tangent (tan δ), has been addressed in several works. Improved preparation methods such as a wet chemical route,[19] chemical combustion,[20] modified solid state reaction,[6] spark plasma sintering,[21] and quick quenching[22] were used to prepare high-performance CCTO ceramics. Additionally, substitution of metal ions into the CCTO lattice can also improve both the dielectric and nonlinear electrical properties of these materials. In recent years, improved dielectric properties with high ε' and very low tan δ were achieved in single- and co-doped CCTO ceramics.[1−10] Ni^{2+},[2,16] Mg^{2+},[1] Al^{3+},[5] Ge^{4+},[6] and F^{-}[3] single doped CCTO can exhibit decreased tan δ values while retaining ε' values at very high values. Simultaneously, numerous research groups have suggested that co-substitution of (Sr^{2+}, Ni^{2+}),[4] (Li^{+}, Al^{3+}),[7] (Y^{3+}, Zr^{4+}),[9] and (Y^{3+}, Al^{3+})[8] into the CCTO lattice can improve the dielectric properties by reducing tan δ while the ε' is still high. In some cases, the nonlinear electrical response was related to the electrical properties of GBs and was improved together with the dielectric properties.[4] As reported by Rhouma et al.,[4] incorporation of Ni^{2+} into a Sr^{2+}-doped CCTO ceramic can enhance ε' to ∼4.44 × 10^4. Simultaneously, tan δ was reduced to ∼0.07. According to other work, the substitution of Ge^{4+} into the CCTO structure can improve its dielectric properties, providing a high ε' ∼ 10^5 and low tan δ ∼0.064−0.068.[6] This motivates us to investigate the dielectric properties and electrical response of (Sr^{2+}, Ge^{4+}) co-doped CCTO ceramics in the present study.

In this work, $CaCu_3Ti_4O_{12}$ and $Ca_{0.95}Sr_{0.05}Cu_3Ti_{4-x}Ge_xO_{12}$ ceramics with x = 0 and 0.05 were prepared via a solid−state reaction (SSR) method. The crystal structure and microstructure of all sintered ceramics were systematically studied. Additionally, the first-principles technique was carried out to investigate the most stable sites of Sr^{2+} and Ge^{4+} ions in the CCTO lattice. Experimental details and their results are discussed in subsequent sections.

2. METHODS

2.1. Ceramic Preparation. With an SSR method, $SrCO_3$ (99.5% purity, Cerac), GeO_2 (99.99% purity, Aldrich), $CaCO_3$ (99.0% purity, Sigma-Aldrich), CuO (99.0% purity, Sigma-Aldrich), TiO_2 (99.99% purity, Aldrich), and C_2H_5OH (99.5% purity, RCI Labscan) were used to prepare $CaCu_3Ti_4O_{12}$ and $Ca_{0.95}Sr_{0.05}Cu_3Ti_{4-x}Ge_xO_{12}$ ceramics. First, stoichiometric ratios of all $Ca_{0.95}Sr_{0.05}Cu_3Ti_{4-x}Ge_xO_{12}$ ceramics were mixed in C_2H_5OH. After that, all mixed raw materials were ball-milled at ∼150 rpm for 24 h. Then, the mixed raw materials were heated at ∼90 °C for ∼24 h. The dried precursors were ground. Next, these powders were calcined in air at 850 °C for 12 h. Finally, the resulting powders were again ground until very fine. The obtained $CaCu_3Ti_4O_{12}$ and $Ca_{0.95}Sr_{0.05}Cu_3Ti_{4-x}Ge_xO_{12}$ powders were formed into a disk-shaped bodies using previously reported procedures.[6] These disk-shaped bodies of $CaCu_3Ti_4O_{12}$ and $Ca_{0.95}Sr_{0.05}Cu_3Ti_{4-x}Ge_xO_{12}$ powders were sintered in air at 1060 °C for 3 h. $CaCu_3Ti_4O_{12}$ and $Ca_{0.95}Sr_{0.05}Cu_3Ti_{4-x}Ge_xO_{12}$ ceramics with x = 0 and 0.05 are referred to as CCTO, Sr05, and Sr05Ge05 ceramics, respectively.

2.2. Characterization and Structural Investigation. The crystal structure of all sintered $CaCu_3Ti_4O_{12}$ and $Ca_{0.95}Sr_{0.05}Cu_3Ti_{4-x}Ge_xO_{12}$ ceramics was studied using X-ray diffractometry (XRD, EMPYREAN, PANalytical B.V.). XRD data were collected over the 2θ range of 20−80°. The XRD data were analyzed with the Rietveld technique using X'Pert HighScore Plus V3.0e software. The optimized parameters and coefficients have been published.[6] The microstructure and chemical composition of the grains and GBs of sintered ceramics were investigated using a desktop scanning electron microscope with an energy dispersive X-ray spectrometer (EDS) (MiniSEM, SEC, SNE-4500M). The oxidation states of transition metal elements in $CaCu_3Ti_4O_{12}$ and $Ca_{0.95}Sr_{0.05}Cu_3Ti_{4-x}Ge_xO_{12}$ ceramics were determined using X-ray photoemission spectroscopy (XPS, PHI5000 VersaProbe II, ULVAC-PHI) on Beamline 5.3 at the Synchrotron Light Research Institute (public organization), Nakhon Ratchasima, Thailand. The XPS data were analyzed using PHI MultiPak XPS software.

According to theoretical point of view, the most stable location of both Ge and Sr in the $CaCu_3Ti_4O_{12}$ was studied using density functional theory (DFT) with the Vienna *Ab initio* Simulation Package (VASP).[23] According to the pseudopotential used in the present study, the projector augmented wave method[24] was chosen. For the exchange−correlation functional, the generalized gradient approximation with the Perdew−Burke−Ernzerhof functional[25] was employed. According to the $CaCu_3Ti_4O_{12}$ pseudopotential, the valence states of Ca are 3s, 3p, and 4s. Also, we used the 3p, 3d, and 4s valence states for Cu, 3s, 3p, 3d, and 4s for Ti, and 2s and 2p for O. For dopant elements, the 3d, 4s, and 4p, as well as the 4s, 4p, and 5s states are the valence states of Ge and Sr. The CCTO unit cell is a cubic structure with a lattice constant of 7.459 Å.[11] Additionally, it contains 2 atoms of Ca, 6 atoms of Cu, 8 atoms of Ti, and 24 atoms of O, for a total of 40 atoms. In the current work, we employed 5 × 2 × 1 CCTO supercells with a total of 400 atoms. The 650 eV of energy cutoff for plane wave expansion was carried out. Moreover, 1 × 3 × 5 k-point samplings generated from the Monkhorst−Pack scheme[26] were used. The conjugate-gradient method was chosen for the structural optimization process.

2.3. Dielectric and Electrical Measurements. Sample preparation for dielectric and electrical measurement is presented elsewhere.[16] A KEYSIGHT E4990A was used to test the dielectric properties of all sintered ceramics using an oscillation voltage (V_{rms}) of 500 mV. This measurement was done in over frequency and temperature ranges of 40−10^7 Hz and −140 to 210 °C, respectively. The methodology for calculation of dielectric properties and electrical response has previously been presented.[6]

3. RESULTS AND DISCUSSION

The results of structural and microstructural examinations are given in Table 1. A fundamental crystalline study of all sintered ceramics was performed using an XRD technique. As shown in Figure 1a, a peak attributed to the sample holder (carbon−

Table 1. Structural Data Obtained from the Rietveld Refinement and Mean Grain Size (G) for the CCTO, Sr05, and Sr05Ge05 Ceramics

sample	CCTO	Sr05	Sr05Ge05
a (Å)	7.393(9)	7.395(0)	7.391(4)
R_{exp} (%)	4.307	4.674	6.665
R_p (%)	4.247	4.363	6.254
R_{wt} (%)	5.693	5.788	13.392
GOF	1.747	1.533	4.037
G (μm)	2.18 ± 1.22	3.63 ± 1.07	215.81 ± 90.89

https://dx.doi.org/10.1021/acs.jpcc.0c04484
J. Phys. Chem. C 2020, 124, 20682−20692

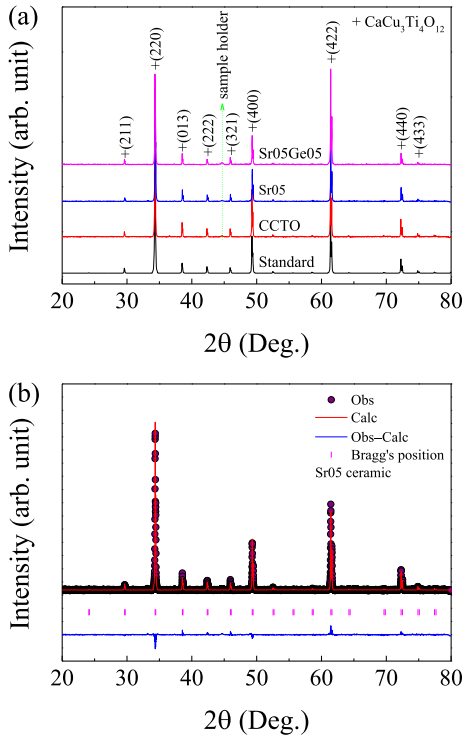

Figure 1. (a) XRD patterns of the CCTO, Sr05, and Sr05Ge05 ceramics compared to a standard X-ray diffractogram. (b) Rietveld profile fit of the Sr05 ceramic.

iron) appeared at $2\theta \approx 44.6-44.8°$, as indicated by a green line. A single-phase of CCTO (JCPDS 75-2188) can be seen in all sintered ceramics. Moreover, it was found that no impurity phases were detected in all samples. The lattice parameters (a) of the CCTO, Sr05, and Sr05Ge05 ceramics were obtained by analyzing the XRD data and employing the Rietveld method. For example, as clearly seen in Figure 1b, the XRD pattern of the Sr05 ceramic was well fitted by the Rietveld refinement approach. Accordingly, the obtained R-factors, for example, the expected R factor (R_{exp}), profile R factor (R_p), and weighted profile R factor (R_{wp}) of all the sintered samples were in the range of 4.2−13.4%. Furthermore, the goodness-of-fit (GOF) factors (∼1.53−4.04) were also obtained. A slightly high R_{wp} and GOF were observed in the Sr05Ge05 ceramic, which may have originated from an abnormal intensity ratio of its XRD pattern because of its preferred orientation.[6] As listed in Table 1, the a values of all sintered ceramics were close to ∼7.391 Å for the lattice constant of CCTO ceramics.[11] Meaningfully, the a value of the Sr05 ceramic is slightly larger than that of the CCTO ceramic. This is owing to the larger ionic radius of the Sr^{2+} than that of the Ca^{2+} host ions. Therefore, substitution of Sr^{2+} into Ca^{2+} sites can cause the a value of CCTO to increase.[27] The addition of Ge^{4+} into the $Ca_{0.95}Sr_{0.05}Cu_3Ti_4O_{12}$ (Sr05Ge05) ceramic leads to decrease of the a value compared to that of the CCTO and Sr05 ceramics. As reported by Shannon,[27] the ionic radius of Ge^{4+} was much smaller than that of Ti^{4+} and other possible sites. Consequently, the decrease in the a value of the Sr05Ge05 ceramic was found.

The microstructure of the sintered ceramics was studied using an scanning electron microscopy (SEM) technique. The obtained SEM images were analyzed using ImageJ software. The microstructure of as-sintered ceramics, simulated flatting surfaces, and grain size distributions of all ceramic samples are shown in Figure 2. Fine-grained microstructure can be seen in the CCTO and Sr05 ceramics. The grain sizes of the Sr05Ge05 ceramic are much larger than those of the two other ceramics. To easily estimate the mean grain size of sintered ceramics, simulated flatting surfaces of all sintered ceramics were created using the hill shade function included in ImageJ software. These results are revealed in Figure 2d−f. As listed in Table 1, the mean grain size of the Sr05 ceramic is slightly larger than that of the CCTO ceramic. A large increase in the grain size can be observed in the Sr05Ge05 ceramic. Furthermore, a bright phase located along the GBs was also found in this ceramic. The mean grain sizes of the CCTO, Sr05, and Sr05Ge05 ceramics were 2.18 ± 1.22, 3.63 ± 1.07, and 215.81 ± 90.89 μm, respectively.

A slight increase in the grain size of the Sr05 ceramic compared to the CCTO ceramic is similar to that reported by Rhouma et al.[4] and Amhil et al.[28] for Sr^{2+}-doped CCTO ceramics. The mean grain size of the $Ca_{0.95}S_{r0.05}Cu_3Ti_4O_{12}$ ceramics can further be enlarged by the addition of a small amount of Ge^{4+} doping ions (Sr05Ge05 ceramic). According to our previous works, for Ge^{4+}-doped CCTO[6] and (Ni^{2+}, Ge^{4+}) co-doped CCTO,[29] the liquid phase sintering mechanism was shown to be the primary origin of the significant expansion of the grain sizes with the addition of a small Ge^{4+} content. In general, a liquid phase can be found along the junction between particles or between GB regions, resulting in an enhanced diffusion rate of ions at the GBs.[6] The liquid-phase source may be due to direct melting of starting materials used (e.g., CuO or GeO_2) and/or by the reaction of starting materials to form a eutectic liquid. However, the melting points of all starting raw materials (>1100 °C) are higher than the sintering temperature (1060 °C), while the eutectic points of CuO−GeO_2 and GeO_2−TiO_2 can occur at 1100 and 1085 °C, respectively.[30,31] The eutectic points of CaO−GeO_2 and SrO−GeO_2 were higher than 1300 °C.[32] It was reported that the eutectic phase of CuO−TiO_2 can be produced at 950 °C in air.[33] Therefore, the liquid phase may have associated with the substitution of Ge into Cu sites of the CCTO lattice at the calcination temperature (850 °C). Then, the eutectic phase of excessed CuO−TiO_2 was formed at 950 °C.[29,33] Therefore, the grain size was significantly enlarged.

The chemical composition of the grains and GBs of the Sr05Ge05 ceramic were studied. As revealed in Figure 3, the amounts of Ca, Cu, Ti, Sr, and Ge detected in the grains and GBs are different. Accordingly, a Cu-rich phase was found at the GBs. A significantly Cu-rich phase was located along with GB layers, as confirmed using the EDS technique. The abundance of a Cu-rich phase at GBs indicates the liquid phase sintering mechanism as a cause of the enormous expansion of grain sizes in the Sr05Ge05 ceramic.[4−6,17,29]

To investigate the most stable position of Ge in the CCTO structure, we first replaced a Ge atom at three different sites, the (1) Ca, (2) Cu, and (3) Ti sites. Ge@Ca refers to the case of a Ca atom substituted by a Ge atom in the CCTO ceramic. Ge@Cu and Ge@Ti structures refer to when Ge atoms occupy Cu and Ti sites, respectively. In the current study, the cohesive energy was calculated by the DFT with the VASP code. The cohesive energy of the Ge atom of these three structures in comparison to the cohesive energy of intrinsic CCTO (E_{coh}) is presented in the inset in Figure 4. It was found that the cohesive energy of Ge@Cu is the highest, followed by Ge@Ca and Ge@Ti, in a descending order. Consequently, the Ge atom is more likely to occupy a Cu site in the CCTO structure.

https://dx.doi.org/10.1021/acs.jpcc.0c04484
J. Phys. Chem. C 2020, 124, 20682−20692

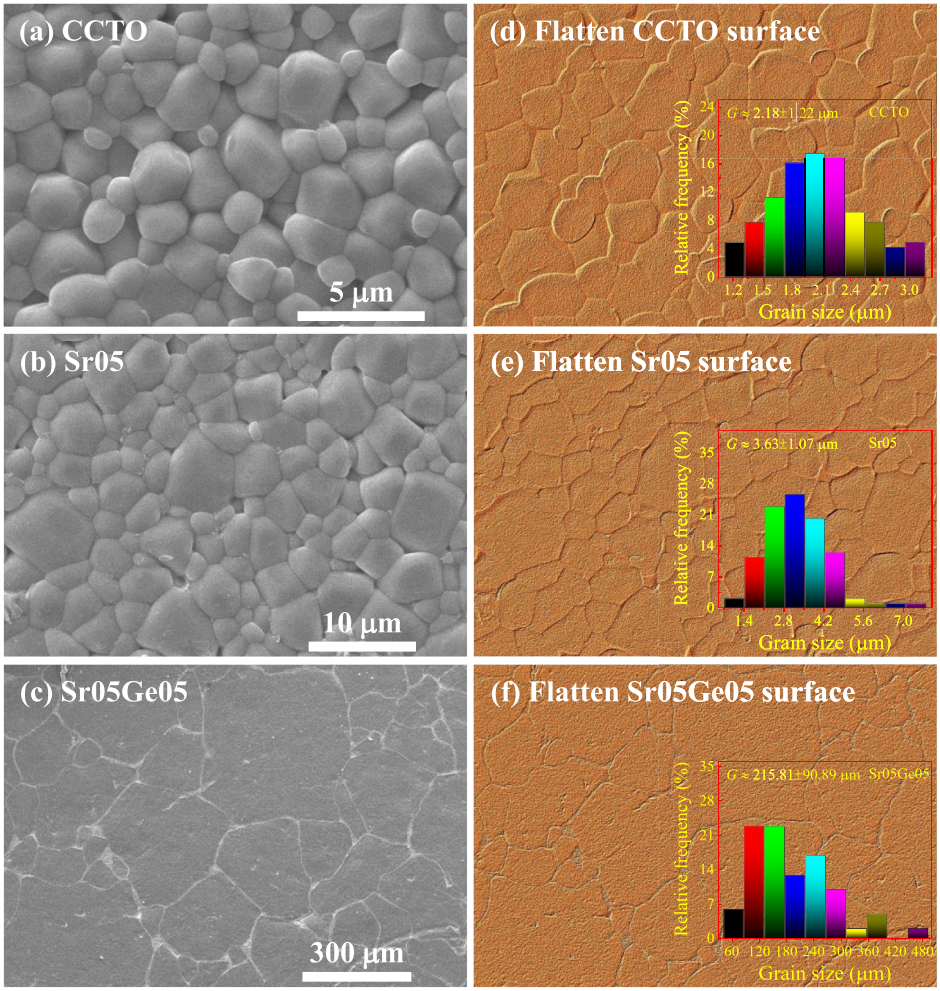

Figure 2. (a−c) SEM images of CCTO, Sr05, and Sr05Ge05 ceramics, respectively. (d−f) Simulated flatting surfaces of these three samples; their insets show grain size distributions of each ceramic.

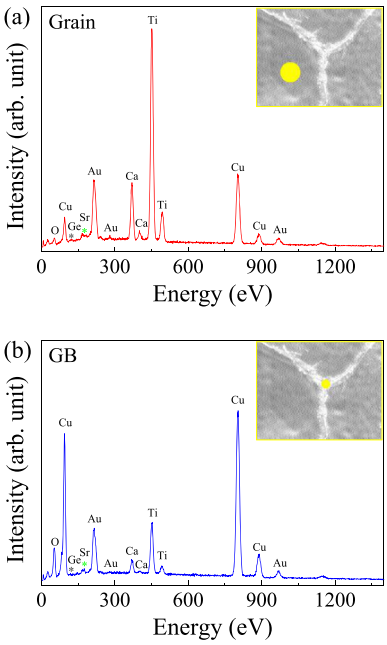

Element	Wt%	At%
O	03.22	10.20
Ge	01.94	01.36
Sr	01.95	01.13
Ca	06.25	07.91
Ti	32.32	34.23
Cu	32.65	26.06
Au	18.27	04.71
Matrix	Correction	ZAF

Element	Wt%	At%
O	06.43	19.73
Ge	00.26	00.17
Sr	00.16	00.09
Ca	01.35	01.66
Ti	06.58	06.74
Cu	65.90	50.91
Au	15.18	03.78
Matrix	Correction	ZAF

Figure 3. EDS spectrum of the Sr05Ge05 ceramic measured at grain and GB regions.

Based on our computational observations, it was confirmed that the replacement of Ge at the Cu sites leads to the release of Cu from the CCTO lattice, forming a Cu-rich phase at the GBs, as clearly seen in Figure 3.

Next, we investigated the most stable location of Sr atoms in Ge-doped CCTO. In the present study, two configurations were considered as shown by structures ***A*** and ***B*** in Figure 4. For structure ***A***, Ge and Sr atoms remained close to each other. In structure ***B***, Sr atoms are rather far from Ge atoms in the CCTO lattice. Both structures are depicted in Figure 4. The total energy obtained from the DFT technique of structure ***A*** is lower than that of structure ***B*** by 34.9 meV. Consequently, the most stable structure for a Ge and Sr co-doped CCTO is structure ***A***. In other words, Ge atoms are likely to stay close to Sr atoms in the CCTO host.

The dielectric and electrical parameters are summarized in Table 2. The frequency dependence of ε' for all sintered ceramics is demonstrated in Figure 5. Clearly, over a frequency range of 40−6 × 10^5 Hz and at 30 °C, the ε' values of the CCTO, Sr05, and Sr05Ge05 ceramics are closely related to the observed SEM images. The IBLC effect has a strong influence on the magnitude of ε' in these three ceramic samples.[1−6] ε' values at 1 kHz and 30 °C of the CCTO, Sr05, and Sr05Ge05 ceramics were 7,618, 11,287, and 69,889, respectively. This result clearly shows enhancement of the giant dielectric response in the (Sr^{2+}, Ge^{4+}) co-doped CCTO ceramic because

https://dx.doi.org/10.1021/acs.jpcc.0c04484
J. Phys. Chem. C 2020, 124, 20682−20692

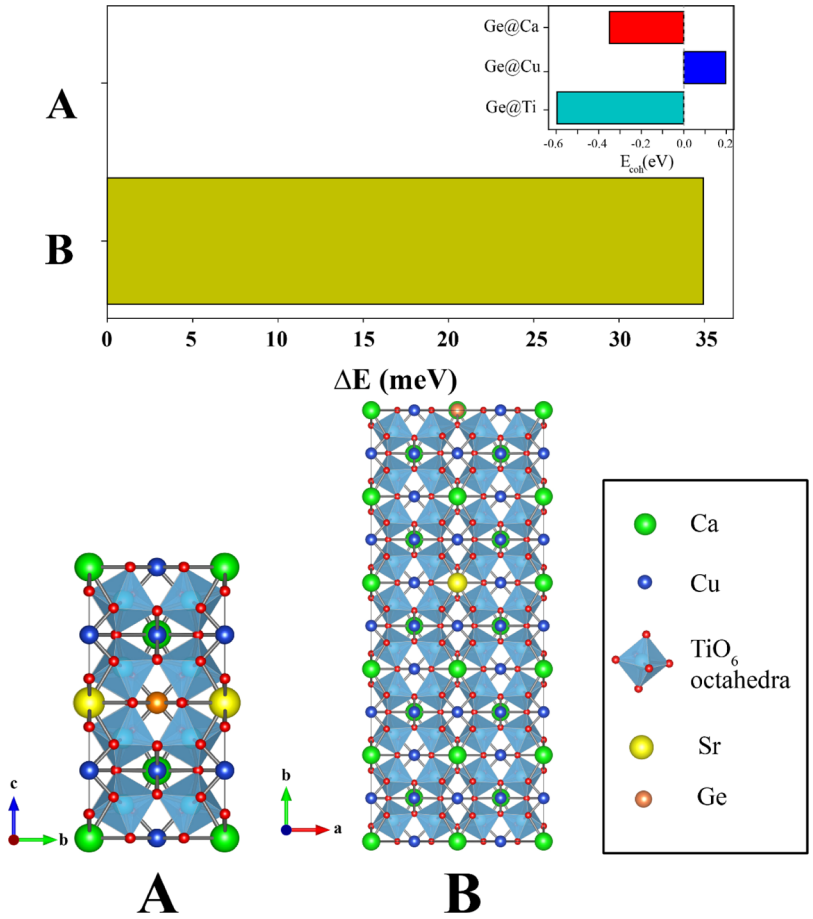

Figure 4. Energy difference of two possible locations of Sr and Ge co-doped CCTO. Configuration A represents the Ge site close to Sr site. The Ge site is far from the Sr site as illustrated in configuration B. The inset shows the cohesive energy of Ge-substituted at Ca, Cu, and Ti sites in the CCTO.

Table 2. ε' and Tan δ at 1 kHz and 30 °C, Experimental Value of R_g at 30 °C, Calculated R_{gb} at 30 °C, Activation Energies of Grains (E_g), and GBs (E_{gb}), Ratios of Cu^+/Cu^{2+} and Ti^{3+}/Ti^{4+} of the CCTO, Sr05, and Sr05Ge05 Ceramics

sample	ε'	tan δ	R_g (Ω·cm)	R_{gb} (Ω·cm)	E_g (eV)	E_{gb} (eV)	Cu^+/Cu^{2+} (%)	Ti^{3+}/Ti^{4+} (%)
CCTO	7618	0.117	63	1.39×10^6	0.133	0.612	25.5/74.5	4.4/95.6
Sr05	11287	0.312	115	1.72×10^5	0.171	0.522	21.5/78.5	4.2/95.8
Sr05Ge05	69889	0.038	27	4.14×10^7	0.137	0.684	24.6/75.4	5.2/94.8

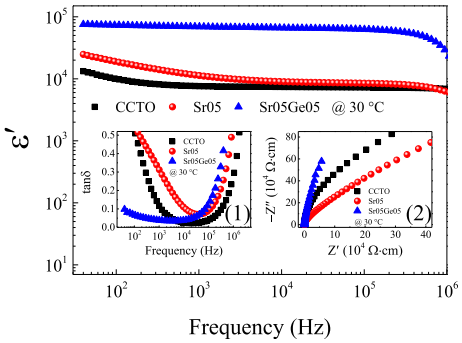

Figure 5. Frequency dependence of ε' at 30 °C of the CCTO, Sr05, and Sr05Ge05 ceramics. Insets (1) and (2) show the frequency dependence of tan δ and the impedance complex Z^* plot at the same temperature.

of microstructural changes.[5] This result is consistent with previous works.[4−6] The frequency dependence of tan δ at 30 °C is illustrated in the inset (1) of Figure 5. Interestingly, the low-frequency tan δ of the Sr05Ge05 ceramic is much smaller than those of the CCTO and Sr05 ceramics. As listed in Table 2, the tan δ values at 1 kHz and 30 °C of the CCTO, Sr05, and Sr05Ge05 ceramics were 0.117, 0.312, and 0.038, respectively. Surprisingly, improved dielectric properties with high ε'∼69,889 and low tan δ ∼0.038 were accomplished in the Sr05Ge05 ceramic. A high tan δ in the CCTO ceramic can be reduced by co-doping with a small concentration of Sr^{2+} and Ge^{4+} ions. Tan δ of the Sr05Ge05 ceramic was significantly decreased even through the mean grain size was greatly enlarged. This observation is rarely found in CCTO-based ceramics. The primary role of Sr^{2+} doping ions is to increase the dielectric properties of CCTO ceramics. As revealed in Figure 2, the mean grain size of the Sr05 ceramic was larger than that of the CCTO ceramic, which is responsible for the observed increase in ε' of the Sr05 ceramic compared to the CCTO ceramic. Unfortunately, tan δ of the CCTO ceramic cannot be reduced by doping with 5 at % Sr. According to our previous work,[6] substitution of 2.5 at % Ge into the Ti site of

https://dx.doi.org/10.1021/acs.jpcc.0c04484
J. Phys. Chem. C 2020, 124, 20682−20692

the CCTO structure can cause an increase in ε' from 6.9×10^4 to 1.1×10^5 because of the significantly enlarged mean grain size from 6.5 to 112.7 μm, while tan δ at 1 kHz decreased from 0.600 to 0.064. In this work, the ε' value of the co-doped Sr05Ge05 ceramic largely increased when compared to both of the CCTO and Sr05 ceramics. This result is consistent with the significant enlargement of the grain size of the Sr05Ge05 ceramic. Thus, one of the important roles of the Ge dopant on the dielectric properties is to enhance the giant dielectric response significantly. Notably, tan δ of the Sr05Ge05 ceramic was significantly reduced compared to both of the CCTO and Sr05 ceramics. Thus, another role of the Ge dopant is to reduce tan δ.

In a case of the undoped CCTO ceramic, tan δ should be inversely proportional to the density of the GB layer/unit volume.[34] According to the impedance spectroscopy analysis for CCTO-based ceramics,[12] the grain boundary resistance (R_{gb}) can be estimated from the diameter of the large semicircle arc of the impedance complex plane (Z^*) plot. By considering the tendency of the impedance complex Z^* plot at 30 °C for all sintered ceramics, as shown in the inset (2) of Figure 5, it was found that the low tan δ in the Sr05Ge05 ceramic is originated from an enhanced R_{gb}.[5] The relationship between tan δ and R_{gb} of CCTO can be well described by the following equation

$$\tan \delta \approx \frac{1}{\omega \varepsilon_0 \varepsilon_s' C_0 R_{gb}} \tag{1}$$

where ω is an angular frequency, ε_0 is the permittivity of free space, ε_s' is a low-frequency dielectric permittivity, and C_0 is a capacitance of free space. This relationship specifies that R_{gb} should be inversely proportional to low-frequency tan δ. According to the research of Mao et al.,[35] the presence of a Cu-rich phase at the GB layer can reduce tan δ to a very low value, ~0.048−0.083, because of improved GB properties. Other studies have reported the same trend as the results of the current work. The presence of a Cu-rich phase and/or other Ge-related insulating phase(s) can enhance the GB resistivity, resulting in a decrease in the low-frequency tan δ value.[5,6,16,22,29] Therefore, the reduction in tan δ of the Sr05Ge05 ceramic was confirmed to be caused by the enhancement of R_{gb}. As revealed in Figure 5, a sharp decrease in ε' and tan δ observed in the CCTO and Sr05 ceramics in the frequency range from 100 Hz to 1 kHz indicates the dominant effect of the sample-electrode interface, which would be evident in the giant dielectric with low R_{gb}.[15]

The dielectric and electrical properties of all ceramic samples were investigated over a wide temperature range of −140 °C to 210 °C. As shown in Figure 6, the low-frequency ε' of the Sr05 ceramic increased with temperature. This dielectric response was a general dielectric behavior of CCTO when it was tested at various temperatures.[1−3,6,10] Nevertheless, for CCTO and Sr05 ceramics, the increase in low-frequency ε' values with temperature is an important factor for contribution to the overall dielectric response. A strong increase in the low-frequency ε' of both CCTO and Sr05 ceramics might be from the influence of the sample-electrode effect.[15] In general, for CCTO, the influence of sample-electrode response is more dominant with low-resistive CCTO ceramics or in states where the R_{gb} of CCTO is significantly reduced, for example, at high temperature or under an applied DC bias.[10,15,36] Lunkenheimer et al.[37] clearly showed that a low-frequency ε' was

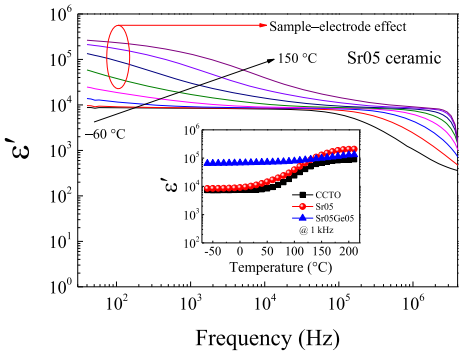

Figure 6. Frequency dependence of ε' for the Sr05 ceramic over a wide temperature range. The inset shows the temperature dependence of ε' at 1 kHz for all sintered ceramics.

dependent on electrode materials (i.e., sputtered Au and Ag). Furthermore, Li et al.[38] demonstrated that the ε' response in the frequency range of 10^2−10^4 Hz can be vanished by changing electrode materials from Au to be In−Ga sputtered electrodes. It was also demonstrated that low-frequency ε' can be changed by preparing electrodes with different methods.[39] The temperature dependence of ε' at 1 kHz of all sintered ceramics is demonstrated in Figure 6. Clearly, the ε' value of the Sr05Ge05 ceramic is more stable with temperature than that of either the CCTO or Sr05 ceramics. The ε' value of the CCTO and Sr05 ceramics increases significantly at temperatures higher than 50 °C. The increased ε' might be primarily caused by the sample-electrode effect.[10] Variation of R_g can be analyzed using the admittance spectroscopy technique. The R_g value is estimated from the frequency dependence of the imaginary part (Y'') of the complex admittance (Y^*) as follows[40]

$$R_g \approx 1/2Y''_{max} \tag{2}$$

where Y''_{max} is the maximum value at the Y''-peak. R_g of all sintered ceramics at 30 °C was calculated and is listed in Table 2. The calculated R_g of CCTO, Sr05, and Sr05Ge05 are 63, 115, and 27 Ω·cm, respectively. The addition of dopants can cause R_g to change slightly. Variation of R_g at various temperatures for the sintered ceramics can be seen in Figure 7a−c. It was found that R_g of all ceramics was reduced with an increasing temperature, which is usually observed in CCTO.[8,12,35] To determine the activation energies of grains (E_g) and GBs (E_{gb}), we used the Arrhenius law as follows

$$R_{g,gb} = R_0 \exp\left(\frac{E_{g,gb}}{k_B T}\right) \tag{3}$$

where R_0 is the pre-exponential term, k_B is the Boltzmann constant, and T is the absolute temperature. However, it is difficult to estimate the R_{gb} value from the Z^* plot because of the sample-electrode effect observed in the CCTO and Sr05 ceramics, as shown in Figure 5. Estimating the R_{gb} value can be made using the electric modulus (M^*) technique.[41] The relationship to calculate the C_{gb} and R_{gb} values using the M^* technique is as follows

$$M^* = j\omega C_0 Z^* = M' + jM'' \tag{4}$$

$$M''_{max} = C_0/2C_{gb} \tag{5}$$

$$\omega \tau_{gb} = \omega R_{gb} C_{gb} = 1 \tag{6}$$

https://dx.doi.org/10.1021/acs.jpcc.0c04484
J. Phys. Chem. C 2020, 124, 20682−20692

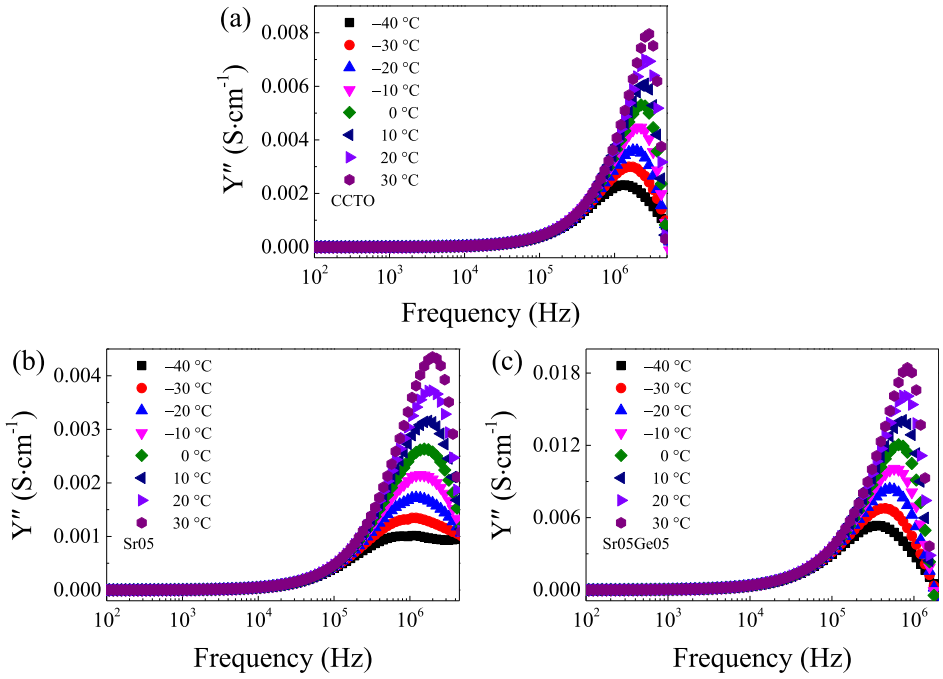

Figure 7. Frequency dependence of Y'' over the temperature range of −40 to 30 °C of (a) CCTO, (b) Sr05, and (c) Sr05Ge05 ceramics.

where M''_{max} is the maximum value of the peak of the imaginary part (M''-peak) of M^*, $\tau_{gb} = 1/2\pi f_{max}$ is the variation relaxation time, and f_{max} is the relaxation frequency. The frequency dependence of M' and M'' for the CCTO, Sr05, and Sr05Ge05 ceramics is given in Figure 8a−c. The trends of change in M''-peak positions are closely related to the step increase in the M' value at the same frequency. These M^* plots show the electrical response of GBs in the undoped and doped CCTO ceramics.[42] The M''-peak position of all samples shifted to a higher frequency with increased temperature. This modulus behavior indicates a decrease in R_{gb} with an increased temperature, which agrees with previously published results.[8,12,19]

The temperature dependence of R_g (solid symbols) and R_{gb} (open symbols) satisfies the Arrhenius law as revealed in Figure 9. The E_g and E_{gb} can be calculated from the slopes of the fitted (red) lines. As summarized in Table 2, the E_g values of the CCTO, Sr05, and Sr05Ge05 ceramics were 0.133, 0.171, and 0.137 eV, respectively. The E_{gb} values of these three ceramics were calculated using eq 3. They were found to be 0.612, 0.522, and 0.684 eV for the CCTO, Sr05, and Sr05Ge05, respectively. As listed in Table 2, the large difference between E_g and E_{gb} relates to the domination of the IBLC effect in these ceramic samples.[12] Although the substitution of Sr^{2+} into $CaCu_3Ti_4O_{12}$ caused E_{gb} to decrease, the addition of a small Ge^{4+} concentration in the Sr^{2+} doped CCTO ceramic greatly enhanced E_{gb} in the co-doped CCTO ceramic. The enhanced E_{gb} of the Sr05Ge05 ceramic indicates the increase in the potential barrier height at GBs (Φ_B) of this co-doped ceramic.[6] Usually, Φ_B exists in non-Ohmic devices owing to (1) the formation of a metal oxide segregation region or precipitated phases and (2) oxygen enrichment along the GBs.[43] According to the microstructure analysis, the segregation of the Cu-/Ge-rich liquid phases along the GBs can be suggested to be the primary cause of the increase in Φ_B. According to the theoretical calculation, the Ge dopant was likely to stay close to the Sr dopant in the CCTO structure.

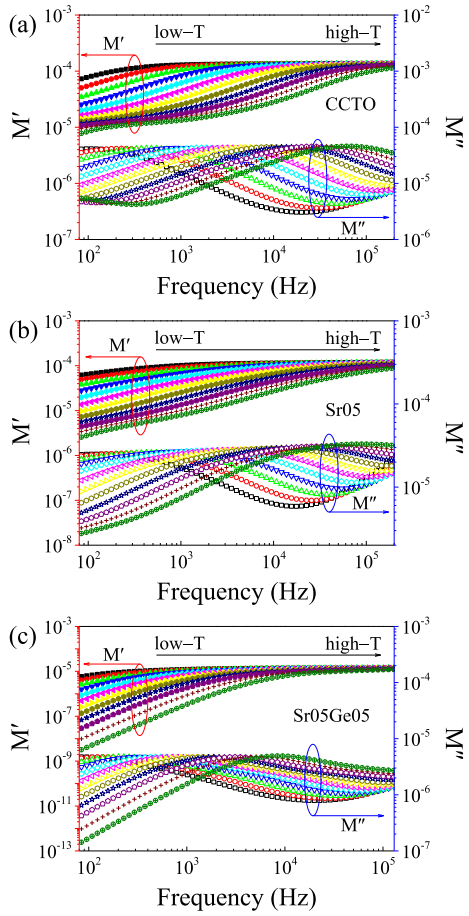

Figure 8. Frequency dependencies of M' and M'' over a wide temperature range for (a) CCTO, (b) Sr05, and (c) Sr05Ge05 ceramics.

The average electronegativity of the Ge and Sr doping ions is higher than that of the Cu and Ca host ions. Thus, oxygen loss

https://dx.doi.org/10.1021/acs.jpcc.0c04484
J. Phys. Chem. C 2020, 124, 20682−20692

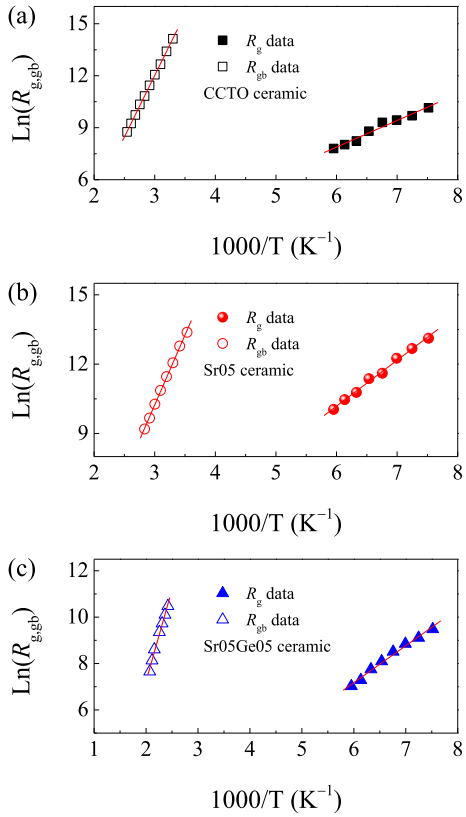

Figure 9. Arrhenius plots of R_g and the estimated R_{gb} values of (a) CCTO, (b) Sr05, and (c) Sr05Ge05 ceramics.

in the Sr05Ge05 ceramic should be lower than that of the CCTO ceramic, giving rise to a higher oxygen concentration at the GBs and hence Φ_B. This improved GB response by a co-doping method agrees with other research studies.[4,8,21,29] R_{gb} at low-temperature can be calculated using E_{gb} data in eq 3. The calculated R_{gb} values at 30 °C of the CCTO, Sr05, and Sr05Ge05 ceramics are listed in Table 2 and are found to be 1.39×10^6, 1.72×10^5, and 4.14×10^7 Ω·cm, respectively. It is worth noting that R_{gb} of the co-doped ceramic enhanced significantly even though the density of the insulating GB layer was reduced by increasing the mean grain size. The significantly increased R_{gb} was resulted by both of the intrinsic and extrinsic effects, which were the increase in Φ_B and formation of the segregation phase(a) along the GBs, respectively. Combining the low-frequency tan δ with the calculated R_{gb} and E_{gb} values, it was found that the decreased low-frequency tan δ might have been caused by the enhanced R_{gb} and E_{gb} values.

Besides the decrease in tan δ, the ε' value of the Sr05Ge05 ceramic increased significantly. According to the back-to-back Schottky potential barrier model, the GB capacitance (C_{gb})/unit area is given by[44]

$$\frac{C_{gb}}{S} = \sqrt{\left(\frac{q\varepsilon' N_d}{8\Phi_B}\right)} \tag{7}$$

where S is the area of the GB perpendicular to the applied electric field, which is estimated to be the grain size, q is the electronic charge, ε' is the dielectric permittivity of the grains, and N_d is the concentration of free charges in the grains. As listed in Table 2, R_g of the Sr05Ge05 ceramic was much less than that of the CCTO and Sr05 ceramics by a factor of >2, indicating a smaller N_d value of the co-doped ceramic. By considering the E_{gb} values, Φ_B increased slightly. Obviously, the mean grain size (~S) of the co-doped ceramic was significantly enlarged. According to eq 7, the largely increased ε' value of the Sr05Ge05 ceramic should be associated with the enhanced N_d and S parameters, which are the intrinsic and extrinsic parameters of the GBs, respectively.

The XPS technique was used to study the charge states of the CCTO, Sr05, and Sr05Ge05 samples. The XPS spectra of Cu and Ti ions of all samples are displayed in Figure 10. Figure

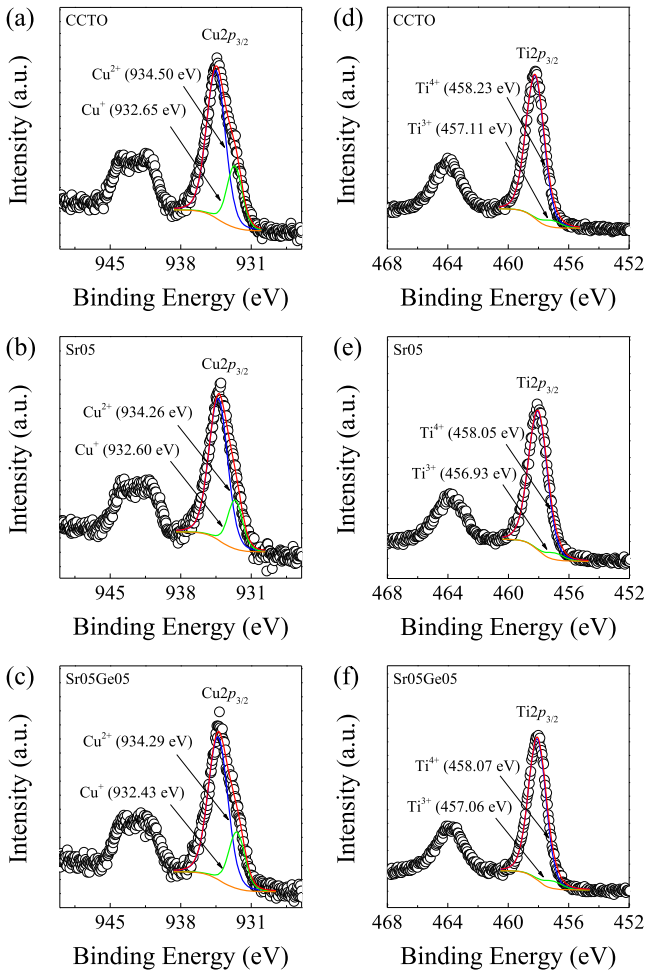

Figure 10. XPS spectra of Cu and Ti ions of all sintered ceramics.

10a−c revealed that all Cu $2p_{3/2}$ peaks have an asymmetric shape that may result from two overlapping peaks of Cu^{2+} and Cu^{+}. The binding energies of Cu^{2+} and Cu^{+} in the XPS spectra were ~934.26−934.50 and ~932.26−932.65 eV, respectively. Simultaneously, the presence of Ti^{3+} was also observed in the XPS spectra, as demonstrated in Figure 10d−f. The binding energies of Ti^{3+} and Ti^{4+} were ~456.93−457.11 and ~458.05−458.23 eV, respectively. Ratios of Cu^{2+}/Cu^{+} and Ti^{4+}/Ti^{3+} are summarized in Table 2. The concentrations of Cu^{+} and Ti^{3+} in the Sr05 ceramic were reduced. This result can be described based on the nonstoichiometry of the Sr analogue of the CCTO ceramics.[45] Accordingly, a slight reduction of $Cu^{2+} \rightarrow Cu^{+}$ due to the instability of Cu^{2+} on heating at >1000 °C is electrically compensated by the slight substitution of excess Ti^{4+} on the Cu site. Then, Cu^{+} oxidized to Cu^{2+} on cooling. Considering the Ca and Cu sites, the charge compensations in

https://dx.doi.org/10.1021/acs.jpcc.0c04484
J. Phys. Chem. C 2020, 124, 20682−20692

the un-doped CCTO ceramic on heating occurred, according to

$$Ca^{2+} + 6Cu^{2+} \rightarrow Ca^{2+} + 4Cu^{+} + 2Ti^{4+} \quad (8)$$

$$Ca^{2+} + 4Cu^{+} + 2Ti^{4+} \rightarrow Ca^{2+} + 2Cu^{+} + 2Cu^{2+} + 2Ti^{3+} \quad (9)$$

In the case of $SrCu_3Ti_4O_{12}$,[45] more Ti occupied on the Cu site and compensated by Sr vacancies (V''_{Sr}). The valence state of Ti^{4+} in the Cu sites unchanged, according to

$$Sr^{2+} + 6Cu^{2+} \xrightarrow{\text{heating}} Sr^{2+} + 4Cu^{+} + 2Ti^{4} \xrightarrow{\text{cooling}} V''_{Sr} + 4Cu^{2+} + 2Ti^{4+} \quad (10)$$

Doping CCTO with Sr^{2+} (Sr05 ceramic) can cause decreases in Cu^{+} and Ti^{3+} due to the charge compensation by V''_{Sr}. As a result, the Cu^{+}/Cu^{2+} and Ti^{3+}/Ti^{4+} ratios of the Sr05 ceramic were lower than those of the CCTO undoped ceramic. After substitution of Ge^{2+}/Ge^{4+} ions into the Sr-doped CCTO ceramic, the Cu^{+}/Cu^{2+} and Ti^{3+}/Ti^{4+} ratios of the Sr05Ge05 ceramic increased significantly. On heating, Cu^{2+} becomes unstable and reduces to Cu^{+}, which was compensated by occupation of Ti^{4+} and/or Ge^{2+}/Ge^{4+} on the Cu sites, according to

$$Sr^{2+} + 6Cu^{2+} \xrightarrow{\text{heating}} Sr^{2+} + (Ge^{4+} + Ti^{4+} + 4Cu^{+}) \quad (11)$$

$$Sr^{2+} + 7Cu^{2+} \xrightarrow{\text{heating}} Sr^{2+} + (Ge^{2+} + 2Ti^{4+} + 4Cu^{+}) \quad (12)$$

On cooling, an internal redox reaction can occur partially: Cu^{+} oxidized to Cu^{2+} ions. However, according to the theoretical calculation, Sr prefers to stay near Ge. Thus, there was no V''_{Sr} near Ge^{2+}/Ge^{4+} ions. The formation of Ti^{3+} and Cu^{+} is due to the charge compensation, according to

$$Sr^{2+} + [Ge^{4+} + 4Cu^{+} + Ti^{4+}] \xrightarrow{\text{cooling}} Sr^{2+} + (Ge^{4+} + (Ti^{3+} + Cu^{2+}) + 3Cu^{+}) \quad (13)$$

or

$$Sr^{2+} + [Ge^{2+} + 4Cu^{+} + 2Ti^{4+}] \xrightarrow{\text{cooling}} Sr^{2+} + (Ge^{2+} + (2Ti^{3+} + 2Cu^{2+}) + 2Cu^{+}) \quad (14)$$

Accordingly, this mechanism gave rise to the increase in the Cu^{+}/Cu^{2+} and Ti^{3+}/Ti^{4+} ratios for the Sr05Ge05 ceramic.

It was clearly seen that the mixed Cu^{2+}/Cu^{+} and Ti^{4+}/Ti^{3+} are consistent with the R_g of each ceramic. The presence of Cu^{+} and Ti^{3+} in CCTO supports the presence of n-type semiconducting grains in this ceramic. The hopping of charge carriers between $Cu^{+} \leftrightarrow Cu^{2+}$ and $Ti^{3+} \leftrightarrow Ti^{4+}$ might be important sources of the semiconductive behavior of the grains.[6,17,18] Interestingly, the very-low tan δ of the Sr05Ge05 ceramic is not consistent with the concentration of Cu^{+} and Ti^{3+}. In this case, the primary cause of low tan δ might be from the formation of the insulating layer at GBs, resulting in a decrease of the long-range migration of charges, that is, DC conduction.[6,29] In addition to the Cu^{2+}/Cu^{+} and Ti^{4+}/Ti^{3+} ratios, examination of the oxidation states of Ge ions revealed that the Ge^{4+}/Ge^{2+} ratio in the Sr05Ge05 ceramic was 39.4/60.6% [data not shown]. According to our XPS spectra and computational results, we can infer that 60.6% of the Ge^{2+} ions might be located in Cu sites because of a reduction of their oxidation state ($Ge^{4+} \rightarrow Ge^{2+}$). According to the XPS analysis, the deviation of the valence states of Cu^{+}/Cu^{2+} and Ti^{3+}/Ti^{4+} can be well described based on the nonstoichiometry.[45] The remainder 39.4% of Ge^{4+} might substitute on the Ti site because of the same valence state. However, during the sintering process, Ge^{4+} can also occupy on the Cu site because of a slight reduction of Cu^{2+} to Cu^{+}. As we have mentioned, the Sr and Ge dopants located at the GBs can suppress oxygen loss, giving rise to the enhanced Φ_B value for the Sr05Ge05 ceramic.

4. CONCLUSIONS

The electronic, dielectric properties, and electrical response of undoped and (Sr^{2+}, Ge^{4+}) co-doped CCTO ceramics were studied entirely. A single-phase of CCTO can be detected in all ceramics. Theoretical and XPS results show that Ge ions are likely substituted into Cu sites, causing a large decomposition of related Cu phases. Grains of the (Sr^{2+}, Ge^{4+}) co-doped CCTO ceramic are the largest in size. Enhanced dielectric permittivity, ~69889, with a reduced loss tangent, ~0.038, is achieved in this ceramic sample. Improved dielectric properties in the (Sr^{2+}, Ge^{4+}) co-doped CCTO ceramic might be associated with an enhanced GB response due to the creation of liquid metastable phases at GB layers. Electron hopping between $Cu^{+} \leftrightarrows Cu^{2+}$ and $Ti^{3+} \leftrightarrows Ti^{4+}$ might be a cause of the semiconductive behavior of the grains. All the results of the current study support the hypothesis of an IBLC as the primary origin of the giant dielectric response in CCTO-based ceramics.

■ AUTHOR INFORMATION

Corresponding Author

Pornjuk Srepusharawoot − *KKU Research Program, Department of Physics, Faculty of Science and Institute of Nanomaterials Research and Innovation for Energy (IN-RIE), NANOTEC-KKU RNN on Nanomaterials Research and Innovation for Energy, Khon Kaen University, Khon Kaen 40002, Thailand*; orcid.org/0000-0001-7216-9778; Email: spornj@kku.ac.th

Authors

Jakkree Boonlakhorn − *KKU Research Program, Department of Physics, Faculty of Science, Khon Kaen University, Khon Kaen 40002, Thailand*

Narong Chanlek − *Synchrotron Light Research Institute (Public Organization), 111 University Avenue, Nakhon Ratchasima 30000, Thailand*

Prasit Thongbai − *KKU Research Program, Department of Physics, Faculty of Science and Institute of Nanomaterials Research and Innovation for Energy (IN-RIE), NANOTEC-KKU RNN on Nanomaterials Research and Innovation for Energy, Khon Kaen University, Khon Kaen 40002, Thailand*

Complete contact information is available at: https://pubs.acs.org/10.1021/acs.jpcc.0c04484

Notes

The authors declare no competing financial interest.

https://dx.doi.org/10.1021/acs.jpcc.0c04484
J. Phys. Chem. C 2020, 124, 20682−20692

■ ACKNOWLEDGMENTS

We would like to acknowledge the National Research Council of Thailand for its financial support. This work has been partially supported by the Research Network NANOTEC (RNN) program of the National Nanotechnology Center (NANOTEC), NSTDA, Ministry of Higher Education, Science, Research, and Innovation (MHESI) and Khon Kaen University, Thailand. This work has received a scholarship under the Post-Doctoral Training Program from Khon Kaen University, Thailand.

■ REFERENCES

(1) Sun, L.; Zhang, R.; Wang, Z.; Cao, E.; Zhang, Y.; Ju, L. Microstructure and enhanced dielectric response in Mg doped $CaCu_3Ti_4O_{12}$ ceramics. *J. Alloys Compd.* **2016**, *663*, 345−350.

(2) Sun, L.; Zhang, R.; Wang, Z.; Cao, E.; Zhang, Y.; Ju, L. Microstructure, dielectric properties and impedance spectroscopy of Ni doped $CaCu_3Ti_4O_{12}$ ceramics. *RSC Adv.* **2016**, *6*, 55984−55989.

(3) Huang, X.; Zhang, H.; Lai, Y.; Li, J. The lowered dielectric loss tangent and grain boundary effects in fluorine-doped calcium copper titanate ceramics. *Appl. Phys. A* **2017**, *123*, 317.

(4) Rhouma, S.; Saîd, S.; Autret, C.; De Almeida-Didry, S.; El Amrani, M.; Megriche, A. Comparative studies of pure, Sr-doped, Ni-doped and co-doped $CaCu_3Ti_4O_{12}$ ceramics: Enhancement of dielectric properties. *J. Alloys Compd.* **2017**, *717*, 121−126.

(5) De Almeida-Didry, S.; Nomel, M. M.; Autret, C.; Honstettre, C.; Lucas, A.; Pacreau, F.; Gervais, F. Control of grain boundary in alumina doped CCTO showing colossal permittivity by core-shell approach. *J. Eur. Ceram. Soc.* **2018**, *38*, 3182−3187.

(6) Boonlakhorn, J.; Thongbai, P.; Putasaeng, B.; Kidkhunthod, P.; Maensiri, S.; Chindaprasirt, P. Microstructural evolution, non-Ohmic properties, and giant dielectric response in $CaCu_3Ti_{4-x}Ge_xO_{12}$ ceramics. *J. Am. Ceram. Soc.* **2017**, *100*, 3478−3487.

(7) Sun, L.; Ni, Q.; Guo, J.; Cao, E.; Hao, W.; Zhang, Y.; Ju, L. Dielectric properties and nonlinear I−V electrical behavior of (Li^{1+}, Al^{3+}) co-doped $CaCu_3Ti_4O_{12}$ ceramics. *Appl. Phys. A* **2018**, *124*, 428.

(8) Du, G.; Wei, F.; Li, W.; Chen, N. Co-doping effects of A-site Y^{3+} and B-site Al^{3+} on the microstructures and dielectric properties of $CaCu_3Ti_4O_{12}$ ceramics. *J. Eur. Ceram. Soc.* **2017**, *37*, 4653−4659.

(9) Xu, Z.; Qiang, H.; Chen, Y.; Chen, Z. Microstructure and enhanced dielectric properties of yttrium and zirconium co-doped $CaCu_3Ti_4O_{12}$ ceramics. *Mater. Chem. Phys.* **2017**, *191*, 1−5.

(10) Hu, P.; Jia, Z.; Shen, Z.; Wang, P.; Liu, X. High dielectric constant and energy density induced by the tunable TiO_2 interfacial buffer layer in PVDF nanocomposite contained with core−shell structured TiO_2@$BaTiO_3$ nanoparticles. *Appl. Surf. Sci.* **2018**, *441*, 824−831.

(11) Subramanian, M. A.; Li, D.; Duan, N.; Reisner, B. A.; Sleight, A. W. High Dielectric Constant in $ACu_3Ti_4O_{12}$ and $ACu_3Ti_3FeO_{12}$ Phases. *J. Solid State Chem.* **2000**, *151*, 323−325.

(12) Sinclair, D. C.; Adams, T. B.; Morrison, F. D.; West, A. R. $CaCu_3Ti_4O_{12}$: One-step internal barrier layer capacitor. *Appl. Phys. Lett.* **2002**, *80*, 2153.

(13) Chung, S.-Y.; Kim, I.-D.; Kang, S.-J. L. Strong nonlinear current−voltage behaviour in perovskite-derivative calcium copper titanate. *Nat. Mater.* **2004**, *3*, 774−778.

(14) Tang, Z.; Huang, Y.; Wu, K.; Li, J. Significantly enhanced breakdown field in $Ca_{1-x}Sr_xCu_3Ti_4O_{12}$ ceramics by tailoring donor densities. *J. Eur. Ceram. Soc.* **2018**, *38*, 1569−1575.

(15) Wu, K.; Huang, Y.; Hou, L.; Tang, Z.; Li, J.; Li, S. Effects of dc bias on dielectric relaxations in $CaCu_3Ti_4O_{12}$ ceramics. *J. Mater. Sci.: Mater. Electron.* **2018**, *29*, 4488−4494.

(16) Boonlakhorn, J.; Putasaeng, B.; Thongbai, P. Origin of significantly enhanced dielectric response and nonlinear electrical behavior in Ni^{2+}-doped $CaCu_3Ti_4O_{12}$: Influence of DC bias on electrical properties of grain boundary and associated giant dielectric properties. *Ceram. Int.* **2019**, *45*, 6944−6949.

(17) Ni, L.; Chen, X. M. Enhancement of Giant Dielectric Response in $CaCu_3Ti_4O_{12}$ Ceramics by Zn Substitution. *J. Am. Ceram. Soc.* **2010**, *93*, 184−189.

(18) Ni, L.; Chen, X. M. Enhanced giant dielectric response in Mg-substituted $CaCu_3Ti_4O_{12}$ ceramics. *Solid State Commun.* **2009**, *149*, 379−383.

(19) Zhang, J.; Zheng, J.; Li, Y.; Liu, Y.; Hao, W.; Lin, L.; Li, Y.; Song, J. Effect of different pH values adjusted by ammonia on the dielectric properties of $CaCu_3Ti_4O_{12}$ ceramics prepared by a sol-gel method. *J. Alloys Compd.* **2019**, *779*, 255−260.

(20) Jumpatam, J.; Thongbai, P. Enhanced dielectric and non-ohmic properties in $CaCu_3Ti_4O_{12}$/$CaTiO_3$ nanocomposites prepared by a chemical combustion method. *J. Mater. Sci.: Mater. Electron.* **2016**, *27*, 12085−12090.

(21) Xu, C.; Zhao, X.; Ren, L.; Sun, J.; Yang, L.; Guo, J.; Liao, R. Enhanced electrical properties of $CaCu_3Ti_4O_{12}$ ceramics by spark plasma sintering: Role of Zn and Al co-doping. *J. Alloys Compd.* **2019**, *792*, 1079−1087.

(22) Li, W.; Tang, L.; Xue, F.; Xin, Z.; Luo, Z.; Du, G. Large reduction of dielectric losses of $CaCu_3Ti_4O_{12}$ ceramics via air quenching. *Ceram. Int.* **2017**, *43*, 6618−6621.

(23) Kresse, G.; Furthmüller, J. Efficiency of ab-initio total energy calculations for metals and semiconductors using a plane-wave basis set. *Comput. Mater. Sci.* **1996**, *6*, 15−50.

(24) Blöchl, P. E. Projector augmented-wave method. *Phys. Rev. B: Condens. Matter Mater. Phys.* **1994**, *50*, 17953−17979.

(25) Perdew, J. P.; Burke, K.; Ernzerhof, M. Generalized Gradient Approximation Made Simple. *Phys. Rev. Lett.* **1996**, *77*, 3865−3868.

(26) Monkhorst, H. J.; Pack, J. D. Special points for Brillouin-zone integrations. *Phys. Rev. B: Condens. Matter Mater. Phys.* **1976**, *13*, 5188−5192.

(27) Shannon, R. D. Revised effective ionic radii and systematic studies of interatomic distances in halides and chalcogenides. *Acta Crystallogr. A* **1976**, *32*, 751−767.

(28) Amhil, S.; choukri, E.; Ben Moumen, S.; Bourial, A.; Essaleh, L. Evidence of large hopping polaron conduction process in strontium doped calcium copper titanate ceramics. *Physica B* **2019**, *556*, 36−41.

(29) Boonlakhorn, J.; Kidkhunthod, P.; Thongbai, P. Significantly improved giant dielectric response in giant dielectric response in $CaCu_{2.95}Ni_{0.05}Ti_{4-x}Ge_xO_{12}$ (x = 0.05, 0.10) ceramics. *Mater. Today Commun.* **2019**, *21*, 100633.

(30) Chen, S.-Y.; Lin, Y.-J. Effect of CuO-based Oxide Additives on Bi_2O_3−ZnO−Nb_2O_5Microwave Ceramics. *Jpn. J. Appl. Phys.* **2001**, *40*, 3305−3310.

(31) Guha, J. P. Subsolidus Equilibria in the System BaO-TiO_2-GeO_2. *J. Am. Ceram. Soc.* **1977**, *60*, 246−249.

(32) Grebenshchikov, R. G.; Shitova, V. I.; Mikirticheva, G. A.; Petrov, S. A.; Grabovenko, L. Y.; Kuchaeva, S. K. Isomorphism and Phase Relationships in the Systems of Metagermanosilicates of Alkaline-Earth Metals. *Russ. J. Appl. Chem.* **2002**, *75*, 1−4.

(33) Lee, S.-Y.; Kim, H. E.; Yoo, S.-I. Subsolidus Phase Relationship in the CaO−CuO−TiO_2 Ternary System at 950°C in Air. *J. Am. Ceram. Soc.* **2014**, *97*, 2416−2419.

(34) Sun, L.; Wang, Z.; Shi, Y.; Cao, E.; Zhang, Y.; Peng, H.; Ju, L. Sol−gel synthesized pure $CaCu_3Ti_4O_{12}$ with very low dielectric loss and high dielectric constant. *Ceram. Int.* **2015**, *41*, 13486−13492.

(35) Mao, P.; Wang, J.; Liu, S.; Zhang, L.; Zhao, Y.; Wu, K.; Wang, Z.; Li, J. Improved dielectric and nonlinear properties of $CaCu_3Ti_4O_{12}$ ceramics with Cu-rich phase at grain boundary layers. *Ceram. Int.* **2019**, *45*, 15082−15090.

(36) Fang, T.-T.; Chung, H.-Y.; Liou, S.-C. Manifestation of the electrode-contact effect on the dielectric response and impedance spectra of $CaSiO_3$-doped $CaCu_3Ti_4O_{12}$. *J. Appl. Phys.* **2009**, *106*, 054106.

(37) Lunkenheimer, P.; Fichtl, R.; Ebbinghaus, S.; Loidl, A. Nonintrinsic origin of the colossal dielectric constants in $CaCu_3Ti_4O_{12}$. *Phys. Rev. B: Condens. Matter Mater. Phys.* **2004**, *70*, 172102.

(38) Li, M.; Shen, Z.; Nygren, M.; Feteira, A.; Sinclair, D. C.; West, A. R. Origin(s) of the apparent high permittivity in $CaCu_3Ti_4O_{12}$ ceramics: clarification on the contributions from internal barrier layer capacitor and sample-electrode contact effects. *J. Appl. Phys.* **2009**, *106*, 104106.
(39) Krohns, S.; Lunkenheimer, P.; Ebbinghaus, S. G.; Loidl, A. Colossal dielectric constants in single-crystalline and ceramic $CaCu_3Ti_4O_{12}$ investigated by broadband dielectric spectroscopy. *J. Appl. Phys.* **2008**, *103*, 084107.
(40) Jumpatam, J.; Somphan, W.; Boonlakhorn, J.; Putasaeng, B.; Kidkhunthod, P.; Thongbai, P.; Maensiri, S. Non-Ohmic Properties and Electrical Responses of Grains and Grain Boundaries of $Na_{1/2}Y_{1/2}Cu_3Ti_4O_{12}$ Ceramics. *J. Am. Ceram. Soc.* **2017**, *100*, 157−166.
(41) Kim, H. E.; Choi, S.-M.; Hong, Y.-W.; Yoo, S.-I. Improved dielectric properties of the $CaCu_3Ti_4O_{12}$ composites using $BaTiO_3$-coated powder as precursor. *J. Alloys Compd.* **2014**, *610*, 594−599.
(42) Peng, Z.; Liang, P.; Chen, X.; Yang, Z.; Chao, X. High thermal stability and excellent dielectric properties of a novel X8R-type $CdCu_3Ti_4O_{12}$ ceramics through a sol-gel technique. *Mater. Res. Bull.* **2018**, *98*, 340−348.
(43) Bueno, P. R.; Leite, E. R.; Oliveira, M. M.; Orlandi, M. O.; Longo, E. Role of oxygen at the grain boundary of metal oxide varistors: A potential barrier formation mechanism. *Appl. Phys. Lett.* **2001**, *79*, 48−50.
(44) Adams, T.; Sinclair, D.; West, A. Characterization of grain boundary impedances in fine- and coarse-grained $CaCu_3Ti_4O_{12}$ ceramics. *Phys. Rev. B: Condens. Matter Mater. Phys.* **2006**, *73*, 094124.
(45) Li, J.; Subramanian, M. A.; Rosenfeld, H. D.; Jones, C. Y.; Toby, B. H.; Sleight, A. W. Clues to the Giant Dielectric Constant of $CaCu_3Ti_4O_{12}$ in the Defect Structure of "$SrCu_3Ti_4O_{12}$". *Chem. Mater.* **2004**, *16*, 5223−5225.

https://dx.doi.org/10.1021/acs.jpcc.0c04484
J. Phys. Chem. C 2020, 124, 20682−20692